

Modeling and simulation of the optical response rod-functionalized reflective surfaces

T. I. Zohdi

Received: 23 March 2012 / Accepted: 15 April 2012
© Springer-Verlag 2012

Abstract In a variety of emerging energy applications such as photovoltaic conversion, thermo-electric conversion, electrochromic actuation, artificial photosynthesis, etc., the capture and trapping of light on a surface is a critical first step in a multistage process. The functionalization of a surface by adding small-scale features, such as fine-scale rods, to trap incoming light, is one possible approach. In this paper, a model that is amenable to large-scale computation is developed. The approach provides a computational tool that allows analysts to quickly study a wide variety of rod-like microstructures. Both analytical and large-scale computational results are presented.

Keywords Surface functionalization · Rod-like microstructure · Light-capture

1 Introduction

The main application of interest in this work is the modeling and simulation of the optical response of surfaces that have been modified (“functionalized”) with rod-like microstructures to absorb light. The absorption of light is a critical step in a multi-stage process of harnessing light for emerging energy conversion technologies, such as photovoltaic conversion, thermo-electric conversion, artificial photosynthesis, etc. More applications are discussed in the concluding remarks of this paper. There are a variety of industrial techniques for surface functionalization, and we refer the reader to Guenther [5], Hawkeye and Brett [6], Macleod [8], Messier et al. [11] and the surveys of the state of the art found in Martin [9] and [10].

In this work, we only focus on the absorption of optical wave-length energy, and do not address the subsequent processes that harness the captured light. Specifically, the characterization of the flow of optical energy, the irradiance, through such systems is the primary objective. It is assumed that the rods and surface features are at least an order of magnitude larger than the wavelength of the incident electromagnetic radiation, therefore “geometrical” ray tracing theory is applicable. Resolving diffraction, for the applications of interest here (which ray theory is incapable of describing) is of secondary importance to the overall propagation of energy (which ray theory captures quite well). Ray-tracing is particularly well-suited to the analysis of such systems. For review of the state-of-the-art in ray-tracing, see Gross [4]. Generally, the interest here is on behavior of initially coherent beams (Fig. 1), composed of multiple collinear (collimated) rays (initially forming a planar wave front), where each ray is a vector in the direction of the flow of electromagnetic energy (the rays are parallel to the initial wave’s propagation vector (Fig. 1)).

Ray-tracing is a method that is employed to produce rapid approximate solutions to wave-equations for high-frequency/small-wavelength applications. Essentially, ray-tracing methods proceed by initially representing wave fronts by an array of discrete rays. *Thereafter, the problem becomes one of an essentially geometric character*, where one tracks the changing trajectories and magnitudes of individual rays which are dictated by the Fresnel conditions (if a ray encounters a material interface). Ray-tracing methods are well-suited for computation of scattering in complex systems that are difficult to mesh/discretize, relative to procedures such as the Finite Difference Time Domain Method or the Finite Element Method and, therefore, they are frequently employed by analysts in such situations.

This paper investigates the sensitivity of high frequency electromagnetic energy propagation, the irradiance, through

T. I. Zohdi (✉)
Department of Mechanical Engineering, University of California,
6195 Etcheverry Hall, Berkeley, CA 94720-1740, USA
e-mail: zohdi@me.berkeley.edu

systems of multiple rod-like scatterers. The current work builds on studies of ray propagation through particulate media by Zohdi [15–18]. It is assumed that the length-scale of the surface features of the rods are large enough, relative to the optical wavelength, that the reflections are specular (coherent) and not diffuse, thus allowing ray tracing theory to be employed. Specifically, the regimes of interest are where the scatterers and surface features are larger than visible light rays: $3.8 \times 10^{-7} m \leq \lambda \leq 7.8 \times 10^{-7} m$. Thus, the rods in this analysis are assumed to possess diameters larger than approximately $10^{-5} m$ (10μ). Ray tracing theory is employed, under the assumption that the surface features of the rods are large enough, relative to the ray wavelength, that such a framework is justified. For rod-like systems smaller than this, one can simply use the ensuing results as rough qualitative guides.

Remark Other high frequency applications where ray-tracing could be used include: (a) regimes where the scatterers and surface features are larger than ultraviolet rays ($10^{-9} m \leq \lambda \leq 10^{-8} m$), (b) regimes where the scatterers and surface features are larger than X-rays ($10^{-11} m \leq \lambda \leq 10^{-9} m$), and (c) regimes where the scatterers and surface features are larger than gamma-rays ($10^{-12} m \leq \lambda \leq 10^{-11} m$).

2 Background: electromagnetic waves

The propagation of electromagnetic waves in free space can be described by a simplified form of Maxwell’s equations

$$\nabla \times \mathbf{E} = -\mu_o \frac{\partial \mathbf{H}}{\partial t}, \quad \text{and} \quad \nabla \times \mathbf{H} = \epsilon_o \frac{\partial \mathbf{E}}{\partial t}, \quad (2.1)$$

where $\nabla \cdot \mathbf{H} = 0$, $\nabla \cdot \mathbf{E} = 0$, \mathbf{E} is the electric field intensity, \mathbf{H} is the magnetic flux intensity, ϵ_o is the free space permittivity and μ_o is the free space permeability. Using standard vector identities, one can show that

$$\begin{aligned} \nabla \times (\nabla \times \mathbf{E}) &= -\mu_o \epsilon_o \frac{\partial^2 \mathbf{E}}{\partial t^2}, \quad \text{and} \\ \nabla \times (\nabla \times \mathbf{H}) &= -\mu_o \epsilon_o \frac{\partial^2 \mathbf{H}}{\partial t^2}, \end{aligned} \quad (2.2)$$

and that

$$\nabla^2 \mathbf{E} = \frac{1}{c^2} \frac{\partial^2 \mathbf{E}}{\partial t^2}, \quad \text{and} \quad \nabla^2 \mathbf{H} = \frac{1}{c^2} \frac{\partial^2 \mathbf{H}}{\partial t^2}, \quad (2.3)$$

where the speed of electromagnetic waves is $c = \frac{1}{\sqrt{\epsilon_o \mu_o}}$. All electromagnetic radiation travels, in a vacuum, at the speed $c \approx 2.99792458 \times 10^8 \pm 1.1 m/s$. In any another medium $v = \frac{1}{\sqrt{\epsilon \mu}}$ for electromagnetic waves.¹

¹ The free space electric permittivity is $\epsilon_o = \frac{1}{c^2 \mu_o} = 8.8542 \times 10^{-12} CN^{-1}m^{-1}$ and the free space magnetic permeability is $\mu_o = 4\pi \times 10^{-7} WbA^{-1}m^{-1} = 1.2566 \times 10^{-6} WbA^{-1}m^{-1}$.

2.1 Plane harmonic waves and ray representations

Now consider the special case of plane harmonic waves, for example of the form

$$\mathbf{E} = \mathbf{E}_o \cos(\mathbf{k} \cdot \mathbf{r} - \omega t) \quad \text{and} \quad \mathbf{H} = \mathbf{H}_o \cos(\mathbf{k} \cdot \mathbf{r} - \omega t), \quad (2.4)$$

where \mathbf{r} is an initial position vector to the wave front, where \mathbf{k} is the direction of propagation. For plane waves, $\mathbf{k} \cdot \mathbf{r} = \text{constant}$. We refer to the phase as $\phi = \mathbf{k} \cdot \mathbf{r} - \omega t$, and $\omega = \frac{2\pi}{\tau}$ as the angular frequency, where τ is the period. For plane waves, the wave front is a plane on which ϕ is constant, which is orthogonal to the direction of propagation, characterized by \mathbf{k} . In the case of harmonic waves, we have

$$\mathbf{k} \times \mathbf{E} = \mu_o \omega \mathbf{H} \quad \text{and} \quad \mathbf{k} \times \mathbf{H} = -\epsilon_o \omega \mathbf{E}, \quad (2.5)$$

and $\mathbf{k} \cdot \mathbf{E} = 0$ and $\mathbf{k} \cdot \mathbf{H} = 0$. The three vectors, \mathbf{k} , \mathbf{E} and \mathbf{H} constitute a mutually orthogonal triad.² The direction of ray propagation is given by $\frac{\mathbf{E} \times \mathbf{H}}{\|\mathbf{E} \times \mathbf{H}\|}$. The Appendix provides more details on the theory of ray representations of electromagnetic waves.

2.2 Special case: natural (random) electromagnetic energy propagation

Electromagnetic waves travelling through space carry electromagnetic energy which flows in the direction of wave propagation. The energy per unit area per unit time flowing perpendicular to a surface in free space is given by the Poynting vector $\mathbf{S} = \mathbf{E} \times \mathbf{H}$. Since at high-frequencies \mathbf{E} , \mathbf{H} and \mathbf{S} oscillate rapidly, it is impractical to measure instantaneous values of \mathbf{S} directly. Consider the harmonic representations in Eq. 2.4 which leads to $\mathbf{S} = \mathbf{E}_o \times \mathbf{H}_o \cos^2(\mathbf{k} \cdot \mathbf{r} - \omega t)$, and consequently the average value over a longer time interval (\mathcal{T}) than the time scale of rapid random oscillation,

$$\langle \mathbf{S} \rangle_{\mathcal{T}} = \mathbf{E}_o \times \mathbf{H}_o \langle \cos^2(\mathbf{k} \cdot \mathbf{r} - \omega t) \rangle_{\mathcal{T}} = \frac{1}{2} \mathbf{E}_o \times \mathbf{H}_o, \quad (2.6)$$

leading to the definition of the *irradiance*

$$I \stackrel{\text{def}}{=} \langle \|\mathbf{S}\| \rangle_{\mathcal{T}} = \frac{1}{2} \|\mathbf{E}_o \times \mathbf{H}_o\| = \frac{1}{2} \sqrt{\frac{\epsilon_o}{\mu_o}} \|\mathbf{E}_o\|^2. \quad (2.7)$$

Thus, the rate of flow of energy is proportional to the square of the amplitude of the electric field. Furthermore, in isotropic media, which we consider for the remainder of the work, the direction of energy is in the direction of \mathbf{S} and in the same direction as \mathbf{k} . Since I is the energy per unit area per unit time, if we multiply by the “cross-sectional” area of the ray (a_r), we obtain the energy associated with the ray, denoted as $Ia_r = Ia_b/N_r$, where a_b is the cross-sectional

² By combining the relations in Eq. 2.5 one obtains $\|\mathbf{k}\| = \frac{\omega}{c}$.

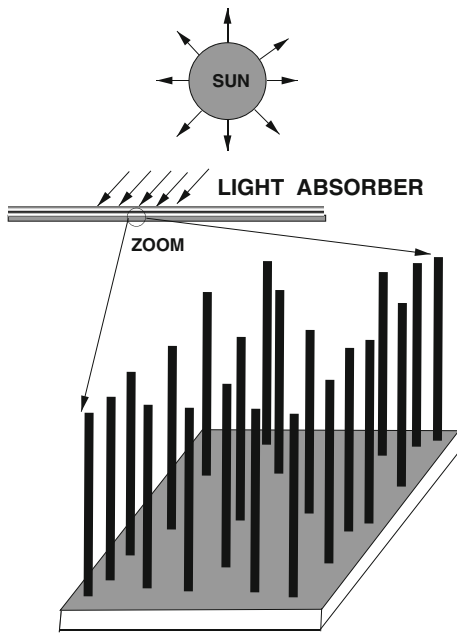


Fig. 1 The scattering system considered, consisting of a beam, comprised of multiple rays, incident on a collection of rod-like scatterers on the surface. The rods are typically grown vertically using silicon, and then coated with materials for the application of interest

area of a beam (comprising all of the rays) and N_r is the number of rays in the beam (see Figs. 1, 8).

2.3 Reflection and absorption of energy

One desirable feature of geometrical ray tracing is that relatively elementary concepts are employed, which we motivate in the next subsection.

2.3.1 Fresnel relations

We consider a plane harmonic wave incident upon a plane boundary separating two different materials, which produces a reflected wave and a transmitted (refracted) wave (Fig. 2). Two cases for the electric field vector are considered: (1) electric field vectors that are parallel (\parallel) to the plane of inci-

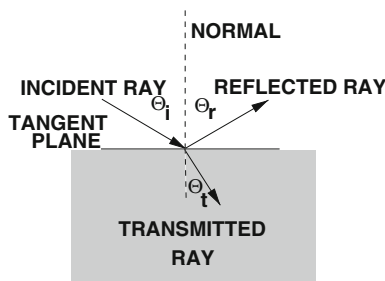


Fig. 2 The nomenclature for Fresnel's equations for an incident ray that encounters an idealized smooth scattering rod

dence and (2) electric field vectors that are perpendicular (\perp) to the plane of incidence. In either case, the tangential components of the electric and magnetic fields are required to be continuous across the interface. Consider case (1). We have the following general vectorial representations

$$\begin{aligned} E_{\parallel} &= E_{\parallel} \cos(\mathbf{k} \cdot \mathbf{r} - \omega t) \mathbf{e}_1 \quad \text{and} \\ H_{\parallel} &= H_{\parallel} \cos(\mathbf{k} \cdot \mathbf{r} - \omega t) \mathbf{e}_2, \end{aligned} \tag{2.8}$$

where \mathbf{e}_1 and \mathbf{e}_2 are orthogonal to the propagation direction \mathbf{k} . By employing the law of refraction ($n_i \sin \theta_i = n_t \sin \theta_t$) we obtain the following conditions relating the incident, reflected and transmitted components of the electric field quantities

$$\begin{aligned} E_{\parallel i} \cos \theta_i - E_{\parallel r} \cos \theta_r &= E_{\parallel t} \cos \theta_t \quad \text{and} \\ H_{\perp i} + H_{\perp r} &= H_{\perp t}. \end{aligned} \tag{2.9}$$

Since, for plane harmonic waves, the magnetic and electric field amplitudes are related by $H = \frac{E}{v\mu}$, we have

$$E_{\parallel i} + E_{\parallel r} = \frac{\mu_i v_i}{\mu_t v_t} E_{\parallel t} = \frac{\mu_i n_t}{\mu_t n_i} E_{\parallel t} \stackrel{\text{def}}{=} \hat{n} E_{\parallel t}, \tag{2.10}$$

where $\hat{\mu} \stackrel{\text{def}}{=} \frac{\mu_t}{\mu_i}$, $\hat{n} \stackrel{\text{def}}{=} \frac{n_t}{n_i}$ and where v_i , v_r and v_t are the values of the velocity in the incident, reflected and transmitted directions.³ By again employing the law of refraction, we obtain the Fresnel reflection and transmission coefficients, generalized for the case of unequal magnetic permeabilities

$$\begin{aligned} r_{\parallel} &= \frac{E_{\parallel r}}{E_{\parallel i}} = \frac{\hat{n} \cos \theta_i - \cos \theta_t}{\hat{n} \cos \theta_i + \cos \theta_t} \quad \text{and} \\ t_{\parallel} &= \frac{E_{\parallel t}}{E_{\parallel i}} = \frac{2 \cos \theta_i}{\cos \theta_i + \frac{\hat{n}}{\mu} \cos \theta_t}. \end{aligned} \tag{2.11}$$

Following the same procedure for case (2), where the components of \mathbf{E} are perpendicular to the plane of incidence, we have

$$\begin{aligned} r_{\perp} &= \frac{E_{\perp r}}{E_{\perp i}} = \frac{\cos \theta_i - \frac{\hat{n}}{\mu} \cos \theta_t}{\cos \theta_i + \frac{\hat{n}}{\mu} \cos \theta_t} \quad \text{and} \\ t_{\perp} &= \frac{E_{\perp t}}{E_{\perp i}} = \frac{2 \cos \theta_i}{\cos \theta_i + \frac{\hat{n}}{\mu} \cos \theta_t}. \end{aligned} \tag{2.12}$$

Our primary interest is in the reflections. We define the reflectances as

$$R_{\parallel} \stackrel{\text{def}}{=} r_{\parallel}^2 \quad \text{and} \quad R_{\perp} \stackrel{\text{def}}{=} r_{\perp}^2. \tag{2.13}$$

³ Throughout the analysis we assume that $\hat{n} \geq 1$.

Particularly convenient forms for the reflections are

$$r_{||} = \frac{\hat{n}^2 \cos \theta_i - (\hat{n}^2 - \sin^2 \theta_i)^{\frac{1}{2}}}{\hat{n}^2 \cos \theta_i + (\hat{n}^2 - \sin^2 \theta_i)^{\frac{1}{2}}} \quad \text{and}$$

$$r_{\perp} = \frac{\cos \theta_i - \frac{1}{\hat{\mu}} (\hat{n}^2 - \sin^2 \theta_i)^{\frac{1}{2}}}{\cos \theta_i + \frac{1}{\hat{\mu}} (\hat{n}^2 - \sin^2 \theta_i)^{\frac{1}{2}}}. \quad (2.14)$$

Thus, the total energy reflected can be characterized by

$$R \stackrel{\text{def}}{=} \left(\frac{E_r}{E_i} \right)^2 = \frac{E_{\perp r}^2 + E_{||r}^2}{E_i^2} = \frac{I_{||r} + I_{\perp r}}{I_i}. \quad (2.15)$$

If the resultant plane of oscillation of the (polarized) wave makes an angle of γ_i with the plane of incidence, then

$$E_{||i} = E_i \cos \gamma_i \quad \text{and} \quad E_{\perp i} = E_i \sin \gamma_i, \quad (2.16)$$

and it follows from the previous definition of I that

$$I_{||i} = I_i \cos^2 \gamma_i \quad \text{and} \quad I_{\perp i} = I_i \sin^2 \gamma_i. \quad (2.17)$$

Substituting these expression back into the expressions for the reflectances yields

$$R = \frac{I_{||r}}{I_i} \cos^2 \gamma_i + \frac{I_{\perp r}}{I_i} \sin^2 \gamma_i = R_{||} \cos^2 \gamma_i + R_{\perp} \sin^2 \gamma_i. \quad (2.18)$$

For natural or unpolarized electromagnetic radiation, the angle γ_i varies rapidly in a random manner, as does the field amplitude. Thus, since

$$\langle \cos^2 \gamma_i(t) \rangle_{\mathcal{T}} = \frac{1}{2} \quad \text{and} \quad \langle \sin^2 \gamma_i(t) \rangle_{\mathcal{T}} = \frac{1}{2}, \quad (2.19)$$

and therefore for natural electromagnetic radiation

$$I_{||i} = \frac{I_i}{2} \quad \text{and} \quad I_{\perp i} = \frac{I_i}{2}. \quad (2.20)$$

and therefore

$$r_{||}^2 = \left(\frac{E_{||r}^2}{E_{||i}^2} \right)^2 = \frac{I_{||r}}{I_{||i}} \quad \text{and} \quad r_{\perp}^2 = \left(\frac{E_{\perp r}^2}{E_{\perp i}^2} \right)^2 = \frac{I_{\perp r}}{I_{\perp i}}. \quad (2.21)$$

Thus, the total reflectance becomes

$$R = \frac{1}{2}(R_{||} + R_{\perp}) = \frac{1}{2}(r_{||}^2 + r_{\perp}^2), \quad (2.22)$$

where $0 \leq R \leq 1$. For the cases where $\sin \theta_i = \frac{\sin \theta_i^*}{\hat{n}} > 1$, one may rewrite reflection relations as

$$r_{||} = \frac{\hat{n}^2 \cos \theta_i - j(\sin^2 \theta_i - \hat{n}^2)^{\frac{1}{2}}}{\hat{n}^2 \cos \theta_i + j(\sin^2 \theta_i - \hat{n}^2)^{\frac{1}{2}}} \quad \text{and}$$

$$r_{\perp} = \frac{\cos \theta_i - \frac{1}{\hat{\mu}} j(\sin^2 \theta_i - \hat{n}^2)^{\frac{1}{2}}}{\cos \theta_i + \frac{1}{\hat{\mu}} j(\sin^2 \theta_i - \hat{n}^2)^{\frac{1}{2}}}, \quad (2.23)$$

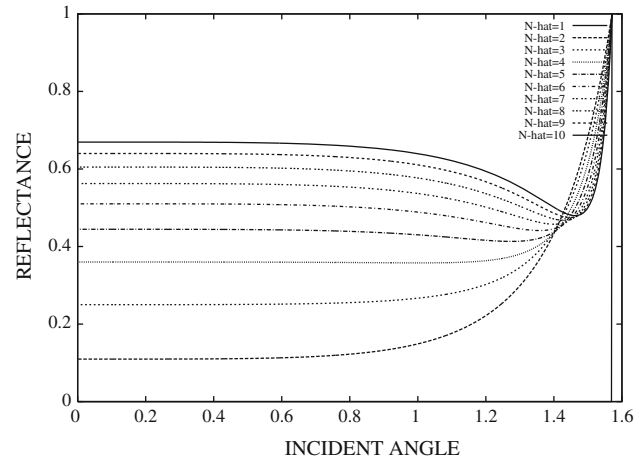


Fig. 3 The reflectance (R) as a function of incident angle

where, $j = \sqrt{-1}$, and in this complex case⁴

$$R_{||} \stackrel{\text{def}}{=} r_{||} \bar{r}_{||} = 1, \quad \text{and} \quad R_{\perp} \stackrel{\text{def}}{=} r_{\perp} \bar{r}_{\perp} = 1, \quad (2.24)$$

where $\bar{r}_{||}$ and \bar{r}_{\perp} are complex conjugates. Thus, for angles above the critical angle θ_i^* , all of the energy is reflected. Notice that as $\hat{n} \rightarrow 1$ we have complete absorption, while as $\hat{n} \rightarrow \infty$ we have complete reflection. The total amount of absorbed power by the rods is $(1 - R)I_i$. Thermal (infrared) coupling effects, which are outside of the scope of this paper, have been accounted for in Zohdi [16].

Remark In order to see the dependency of R on \hat{n} and θ_i we can explicitly write

$$R = \frac{1}{2} \left(\left(\frac{\hat{n}^2 \cos \theta_i - (\hat{n}^2 - \sin^2 \theta_i)^{\frac{1}{2}}}{\hat{n}^2 \cos \theta_i + (\hat{n}^2 - \sin^2 \theta_i)^{\frac{1}{2}}} \right)^2 + \left(\frac{\cos \theta_i - \frac{1}{\hat{\mu}} (\hat{n}^2 - \sin^2 \theta_i)^{\frac{1}{2}}}{\cos \theta_i + \frac{1}{\hat{\mu}} (\hat{n}^2 - \sin^2 \theta_i)^{\frac{1}{2}}} \right)^2 \right). \quad (2.25)$$

Figure 3 illustrates the behavior of R for various \hat{n} , as a function of θ_i . For all but $\hat{n} = 2$, is there discernible nonmonotone behavior. The nonmonotone behavior is slight for $\hat{n} = 4$, but nonetheless present. Clearly, as $\hat{n} \rightarrow \infty$, $R \rightarrow 1$, no matter what the angle of incidence's value. Also, as $\hat{n} \rightarrow 1$, provided that $\hat{\mu} = 1$, $R \rightarrow 0$, i.e. all incident energy is absorbed. With increasing \hat{n} , the angle for minimum reflectance grows larger. For more details, we refer the reader to the cited literature in the references.

2.3.2 Reflectivity

In summary, the angle between the point of contact of a ray (Fig. 2) and the outward normal to the surface at that point

⁴ The limiting case $\frac{\sin \theta_i^*}{\hat{n}} = 1$, is the critical angle (θ_i^*) case.

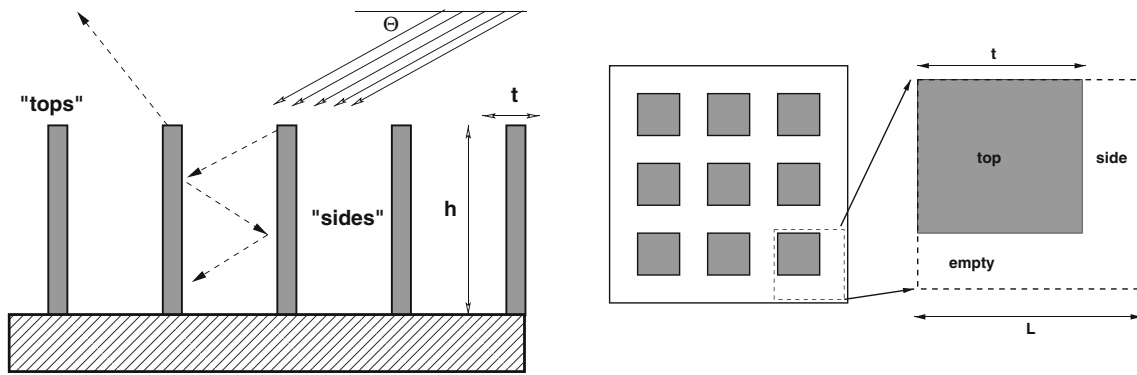


Fig. 4 Parametrized system for optimization. Left side view. Right top view and a single cell

is the angle of incidence (θ_i). The classical reflection law states that the angle at which the ray is reflected is the same as the angle of incidence and that the incoming (incident, θ_i) and outgoing (reflected, θ_r) rays lay in the same plane, and $\theta_i = \theta_r$. Furthermore, refraction law states that, if the ray passes from one medium into a second one (with a different index of refraction), and, if the index of refraction of the second medium is less than that of the first, the angle the ray makes with the normal to the interface is always less than the angle of incidence, where $n \stackrel{\text{def}}{=} \frac{c}{v} = \sqrt{\frac{\epsilon\mu}{\epsilon_o\mu_o}} = \frac{\sin\theta_i}{\sin\theta_t}$, θ_t being the angle of the transmitted ray (Fig. 2), c is the propagation speed in a vacuum and v is the propagation speed in the incident medium. By using the classical Fresnel equations, one can also describe the changes in ray magnitude. Consider a plane harmonic wave incident upon a boundary separating two different materials, which produces a reflected wave and a transmitted (refracted) wave (Fig. 2), the amount of incident electromagnetic energy (I_i) that is reflected (I_r) is given by the total reflectance $R \stackrel{\text{def}}{=} \frac{I_r}{I_i}$, where $0 \leq R \leq 1$ e, R given by Eq. 2.25, for unpolarized electromagnetic radiation, where \hat{n} is the ratio of the refractive indices of the ambient (incident) medium (n_i) and transmitted rod-like medium (n_t), $\hat{n} = n_t/n_i$, where $\hat{\mu}$ is the ratio of the magnetic permeabilities of the surrounding incident medium (μ_i) and transmitted rod-like medium (μ_t), $\hat{\mu} = \mu_t/\mu_i$. We consider applications where the magnetic permeability is, within experimental measurements, virtually the same for both the matrix and rod phases. Thus, for the remainder of the work, we shall take $\hat{\mu} = 1$ ($\mu_o = \mu_i = \mu_t$) and, thus, $\hat{n} = \frac{n_t}{n_i} = \sqrt{\frac{\epsilon_t\mu_t}{\epsilon_i\mu_i}} \Rightarrow \epsilon_t\mu_t = (\hat{n})^2\epsilon_i\mu_i \Rightarrow \epsilon_t = (\hat{n})^2\epsilon_i$, where $\epsilon_i = \epsilon_o$.

Remark From this point forth, we assume that the ambient medium (surrounding the rods) behaves as a vacuum. Accordingly, there are no energetic losses as the rays move through the surrounding medium.⁵ Furthermore, we assume

⁵ Losses could be easily incorporated by using a Beer-Lambert type decay relation.

that refracted rays which enter a rod are not re-emitted. The re-emission problem is quite complex, and involves multiple internal reflections, as well as conversion of electromagnetic energy into heat. It is important to note that multiple internal reflections and re-emission also leads to an immense growth in the number of rays, which is beyond the scope of the present analysis. However, some of these issues have been addressed in Zohdi [16].

3 Analytical trends for periodic media and aligned incidence

3.1 Periodic cell analysis

In order to qualitatively characterize the absorption trends as a function of rods' geometry, we consider a periodic array of (square cross-sectional) rods (the simulations are general, however). The base is assumed to play no role, i.e. it is transparent. Referring to the configuration in Fig. 4, and considering a periodic cell, we define the following:

- An individual incoming ray: I_I^i ,
- An individual reflected ray from the top: $I_R^{top,i} = R(\phi)I_I^i$, where $\phi = \frac{\pi}{2} - \theta$,
- An individual reflected ray, that undergoes M side-wall reflections: $I_R^{side,i} = R^M(\theta)I_I^i$, where $M = \frac{h}{(L-t)\tan\theta}$.

With these definitions, we can characterize, for N_r incoming rays on a cell:

- The total incoming rays: $I_I^{total} = N_r I_I^i$,
- The percentage of reflected rays from the top: $I_R^{top,total} = R(\phi)I_I^i \frac{N_r t^2}{L^2}$,
- The percentage of reflected rays, that undergo m side-wall reflections: $I_R^{side,total} = R^M(\theta)I_I^i \frac{N_r(L-t)t}{L^2}$,
- The percentage of reflected rays, that encounter the empty region: $I_R^{empty,total} = I_I^i \frac{N_r(L-t)L}{L^2}$.

Fig. 5 The behavior with $\hat{n} = 2.5$, $h = L$ and varying θ and t

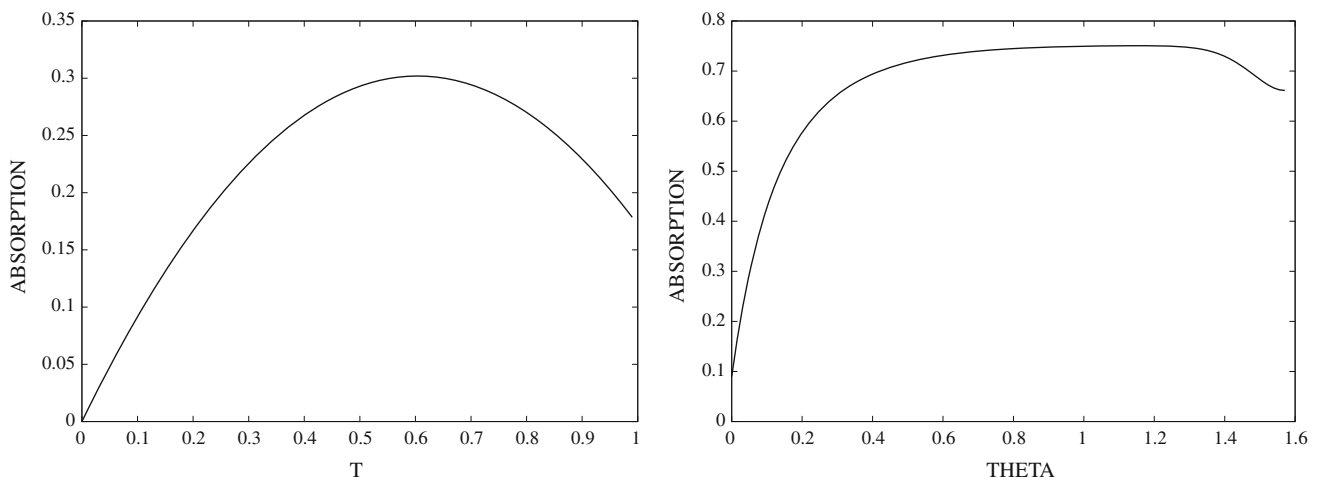
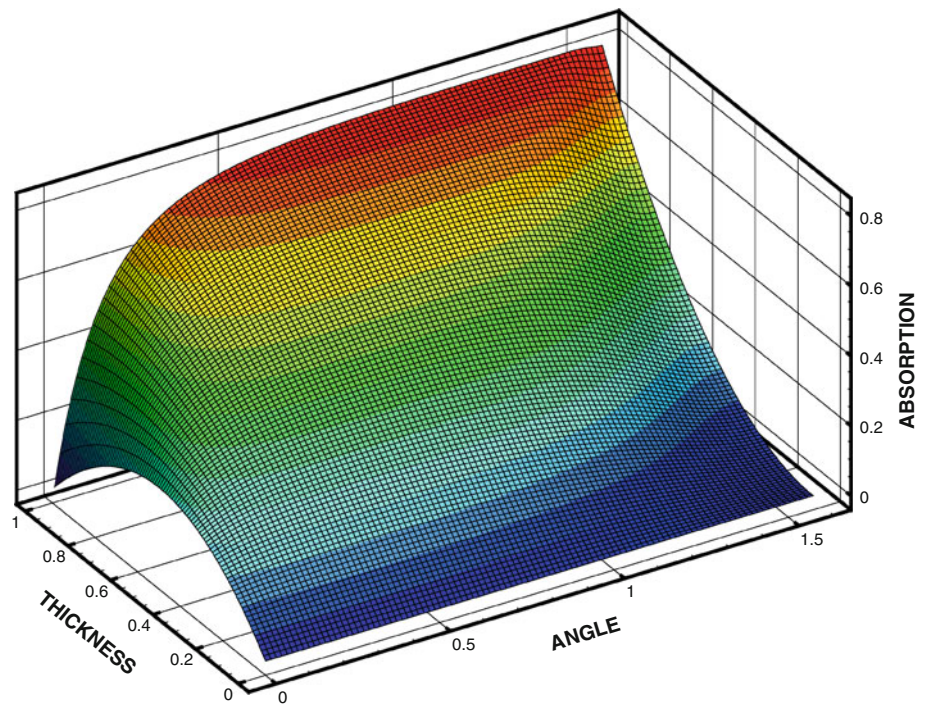


Fig. 6 The behavior with $\hat{n} = 2.5$, $h = L$, *Left* varying t with fixed angle $\theta = \pi/100$ and *right* varying θ with fixed $t = 0.9L$ (these plots are cross-sections of Fig. 5)

The total absorbed by the rods in the periodic cell is:

$$A \stackrel{\text{def}}{=} I_I^{\text{total}} - I_R^{\text{empty,total}} - \left(I_R^{\text{top,total}} + I_R^{\text{side,total}} \right), \tag{3.1}$$

or, explicitly, normalizing A by I_I^{total}

$$\hat{A} \stackrel{\text{def}}{=} \frac{A}{I_I^{\text{total}}} = \frac{t}{L} - \left(\frac{t^2}{L^2} R(\phi) + \left(\frac{t}{L} - \frac{t^2}{L^2} \right) R^M(\theta) \right), \tag{3.2}$$

Carpet plots of $t - \theta$ -dependence of \hat{A} is shown in Fig. 5. Cross-sections of the carpet plot are shown in Fig. 6. The

plots indicate that for very thick systems, and an absorption of near $\hat{A} = 0.8$ is possible, with relative large values of θ . However, the effect drops off for very large θ , because of a decreasing number of side-wall reflections. We note that in the plots, M is treated as a continuous variable.

3.2 Asymptotic cases: absorption as a function of t

There are two asymptotic cases that are of interest:

- (CASE 1) For shallow angles (small θ), there is a unique optimal t . This is due to the competition between

absorption from the tops and intra-rod reflection. Asymptotically, as $\theta \rightarrow 0$, $R(\phi) \rightarrow 1$, $R(\theta) = \left(\frac{\hat{n}-1}{\hat{n}+1}\right)^2 < 1$, $M \rightarrow \infty$

$$\hat{A} \rightarrow \frac{t}{L} \left(1 - \frac{t}{L}\right), \tag{3.3}$$

which has a unique maximizer at $t = \frac{L}{2}$. Plugging in this value yields $\hat{A}(L/2) = 0.25$.

- (CASE 2) For deeper angles, asymptotically, as $\theta \rightarrow \frac{\pi}{2}$, $R(\theta) \rightarrow 1$, $R(\phi) = \left(\frac{\hat{n}-1}{\hat{n}+1}\right)^2 < 1$, $M \rightarrow 0$ there is no optimum; absorption increases with t (the cross-sectional area of the rods)

$$\hat{A} \rightarrow \frac{t}{L} \left(1 - \frac{t}{L}R(\phi)\right), \tag{3.4}$$

until $t = L$.

Remark In order to determine the extremum as a function of t , one computes (noting that $M = M(t)$)

$$\begin{aligned} \frac{\partial \hat{A}}{\partial t} &= \frac{1}{L} - \frac{2t}{L^2}R(\phi) - \frac{1}{L}R^M(\theta) + \frac{2t}{L^2}R^M(\theta) \\ &\quad - \left(\frac{t}{L} - \frac{t^2}{L^2}\right) \left(R^M(\theta) \ln R(\theta) \frac{h}{(L-t)^2 \tan \theta}\right) = 0, \end{aligned} \tag{3.5}$$

which provides a formula for extremum choices of t . Solutions to the above are denoted t^* . If t^* satisfies $\frac{\partial^2 \hat{A}}{\partial t^2} > 0$, then it is a minimizer of \hat{A} , while if t^* satisfies $\frac{\partial^2 \hat{A}}{\partial t^2} < 0$, then it is a maximizer of \hat{A} . Clearly, such an expression allows one to determine the optimal inclination, thus controlling θ for the desired absorption. In order to determine simultaneous extrema pair of θ and t , one can attempt to use Newton’s scheme, forming the Hessian and Gradient and solve for $i = 1, 2, \dots, N$,

$$\begin{bmatrix} \frac{\partial^2 \hat{A}}{\partial t^2} & \frac{\partial^2 \hat{A}}{\partial t \partial \theta} \\ \frac{\partial^2 \hat{A}}{\partial \theta \partial t} & \frac{\partial^2 \hat{A}}{\partial \theta^2} \end{bmatrix} \begin{bmatrix} (t^{i+1} - t^i) \\ (\theta^{i+1} - \theta^i) \end{bmatrix} = - \begin{bmatrix} \frac{\partial \hat{A}}{\partial t} \\ \frac{\partial \hat{A}}{\partial \theta} \end{bmatrix} \tag{3.6}$$

However, because the system may not necessarily have unique minima, the Hessian may not be positive definite, and thus nonconvex optimization techniques may need to be used.

4 General rod-like systems

4.1 Computational algorithms

In order to consider more complex scattering systems, i.e. potentially non-aligned rays, randomly placed rods, etc, we

employ the following computational algorithm to propagate rays is as follows, starting at pseudo-time $t = 0$ and ending at $t = T$:

```

(1) COMPUTE POSSIBLE RAY REFLECTIONS :
(a) CHECK IF A RAY HAS ENCOUNTERED A SURFACE
(b) IF SO, USE THE FRESNEL RELATIONS FOR TRAJECTORY CHANGE :
    (i) COMPUTE SURFACE NORMAL AT CONTACT/SURFACE - INTERSECTION POINT :
        (1) FOR A SURFACE  $\Phi(x_1, x_2, x_3) = 0$  COMPUTE INTERSECTION
        (2) COMPUTE NORMAL  $\mathbf{n} = \frac{\nabla \Phi(x_1, x_2, x_3)}{\|\nabla \Phi(x_1, x_2, x_3)\|}$ 
        (3) COMPUTE REFLECTED ANGLE RELATIVE TO THE NORMAL (IN PLANE)
    (ii) COMPUTE ANGLE CHANGE FOR REFLECTED RAY
(c) COMPUTE ABSORPTION BY RODS AND RAY MAGNITUDE CHANGE
        
$$R = \frac{1}{2} \left( \left( \frac{\frac{\hat{n}^2}{\mu} \cos \theta_i - (\hat{n}^2 - \sin^2 \theta_i)^{\frac{1}{2}}}{\frac{\hat{n}^2}{\mu} \cos \theta_i + (\hat{n}^2 - \sin^2 \theta_i)^{\frac{1}{2}}} \right)^2 + \left( \frac{\cos \theta_i - \frac{1}{\mu} (\hat{n}^2 - \sin^2 \theta_i)^{\frac{1}{2}}}{\cos \theta_i + \frac{1}{\mu} (\hat{n}^2 - \sin^2 \theta_i)^{\frac{1}{2}}} \right)^2 \right),$$

(2) INCREMENT ALL RAY FRONT POSITIONS :
        
$$\mathbf{r}_i(t + \Delta t) = \mathbf{r}_i(t) + \Delta t \mathbf{v}_i(t), \quad i = 1, \dots, \text{RAYS}$$

(3) GO TO (1) AND REPEAT WITH  $(t = t + \Delta t)$ 
    
```

(4.1)

The time-marching, “pseudo-time”, step size Δt is dictated by the size of the rods. A somewhat ad-hoc approach is to scale the time step size according to $\Delta t \propto \frac{\xi b}{\|\mathbf{v}\|}$, where b is the radius of the rods, $\|\mathbf{v}\|$ is the magnitude of the velocity of the rays and ξ is a scaling factor, typically $0.05 \leq \xi \leq 0.1$.

4.2 An example: aligned and mis-aligned rods

In the following examples, the primary quantity of interest is to characterize the response of the irradiance of a beam (circular in cross-section), encountering a collection of rods (of circular cross-section). In the first example, we considered a group of N^{rods} rods, of equal size, on a rectangular domain of dimensions, $D \times D$. The relative (to the surrounding (vacuum) medium) refractive indices of the rods was set to $\hat{n} = 4$, which essentially indicates that each rod is highly reflective. We used $N^{rods} = 25$ rods and $N^{rays} = 1,000$ colinear rays

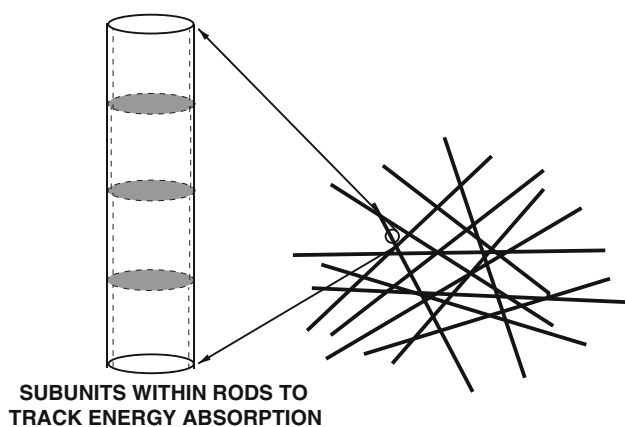


Fig. 7 Subunit (*cylinders*) within a cylindrical rod to track energy absorption along the rods

in the beam, randomly arranged in a circular domain. This system provided stable results, i.e. increasing the number of rays and/or the number of rods beyond these levels resulted in negligibly different overall system responses. The irradiance beam parameter was set to $I_o = ||I(0)||$, which is the magnitude of the initial irradiance at time $t = 0$. The irradiance for each ray was calculated as I_{ab}/N^{rays} . Due to the problem's linearity, it is insensitive to the initial magnitude of I_o (it scales out). We repeatedly refined the number of rays and found no significant difference beyond the 1,000 ray result. Therefore, we consider the responses to be, for all practical purposes, independent of the ray-grid density. This rod/ray system provided stable results, i.e. increasing the number of rays and/or the number of rods surrounding the beam resulted in negligibly different overall system responses. The simulations were run until the rays completely exited the domain, which corresponded to a time-scale on the order of $\frac{D}{c}$. The initial velocity vector for all of the initially co-linear rays comprising the beam was $\mathbf{v}(t = 0) = c(\cos\frac{\pi}{4}, \sin\frac{\pi}{4}, 0)$ (inclined angle of incidence) (Fig. 7). Figure 8 shows successive frames of the rays as they move through the system. Figure 10 illustrates the total energy content in the rays as a function of time. The color of the vectors indicate the irradiance, while the color of the rods indicate the absorption of the irradiant energy. The remaining energy has been absorbed by the rods. At steady-state, 50% of the energy has been absorbed by the aligned system. As a second example, we randomly distributed the 25 cylindrical rods (random directions) as shown in a square beam cross-section (Fig. 9). The initial velocity vector for all of the initially co-linear rays comprising the beam was $\mathbf{v}(t = 0) = (c, 0, 0)$ (direct angle of incidence). Figure 9 shows successive frames of the rays as they move through the system. Figure 10 illustrates the total energy (irradiance) content in the rays as a function of time. It is notable that relative to the the aligned rods case, the misaligned rods case blocks (reflects back) considerably more energy. The remaining energy has been absorbed by the

rods. At steady-state, 75% of the energy has been absorbed by the misaligned system.

5 Concluding remarks

This paper studied optical scattering through a system of rods analytically and numerically. Ray tracing theory was employed, and was justified due to the size of the scatterers relative to the wavelength of incident electromagnetic radiation. It is important to recognize that one can describe the aggregate ray behavior in an even more detailed manner via higher moment distributions of rays, for example employing the skewness, kurtosis, etc. Furthermore, it is important to note that for the ray tracing method, there are two natural ways to proceed to exploit parallelism: (1) By assigning each processor its share of the rays, and checking which scatterers interact with those rays or (2) By assigning each processor its share of scatterers, and checking which rays interact with those scatterers. High-performance computational methods for the determination of ray/rod intersection can be developed by slightly modifying fast ray-rod contact detection algorithms found in, for example, Pöschel and Schwager [12], for general object shapes.

The dramatic rise in readily available computational power has made the implementation and use of the preceding model potentially readily accessible. In closing, we mention a variety of applications for rod-functionalized surfaces that can profit from such a computational tool. A rather obvious application is the optical response of naturally occurring “furry” surfaces, which is clearly of interest in biological studies (Preciado et al. [13]). However, a very closely related topic is the optical response of hair, which has been of interest to the cosmetics industry for many years (Stamm et al. [14]), but with studies that have been limited to experimental studies and/or simple models, due to a lack of computational power. Of concern there is the overall reflectivity of surfaces covered with natural and synthetic hair-like surfaces, as a function of the hair strand density, color, length, angle of inclination, cross-section, surface-treatment and whether the strands are combed or entangled. The presented model is amenable to large-scale computation that can ascertain the response of an entire set of strands (reflecting surfaces) by directly computing the propagation of light rays interacting with the multiple reflecting surfaces. The approach provides a computational tool that allows analysts to quickly study a wide variety of hair-like configurations. Clearly, this tool allows an analyst to compute the reflectivity of a variety of relevant parameter-combinations, which can help in the development of synthetic hair, hair products, etc. This also has implications for the construction of new synthetic hair-like cloaking and signal response masking surface materials. Another application is the reflectivity of composites, which

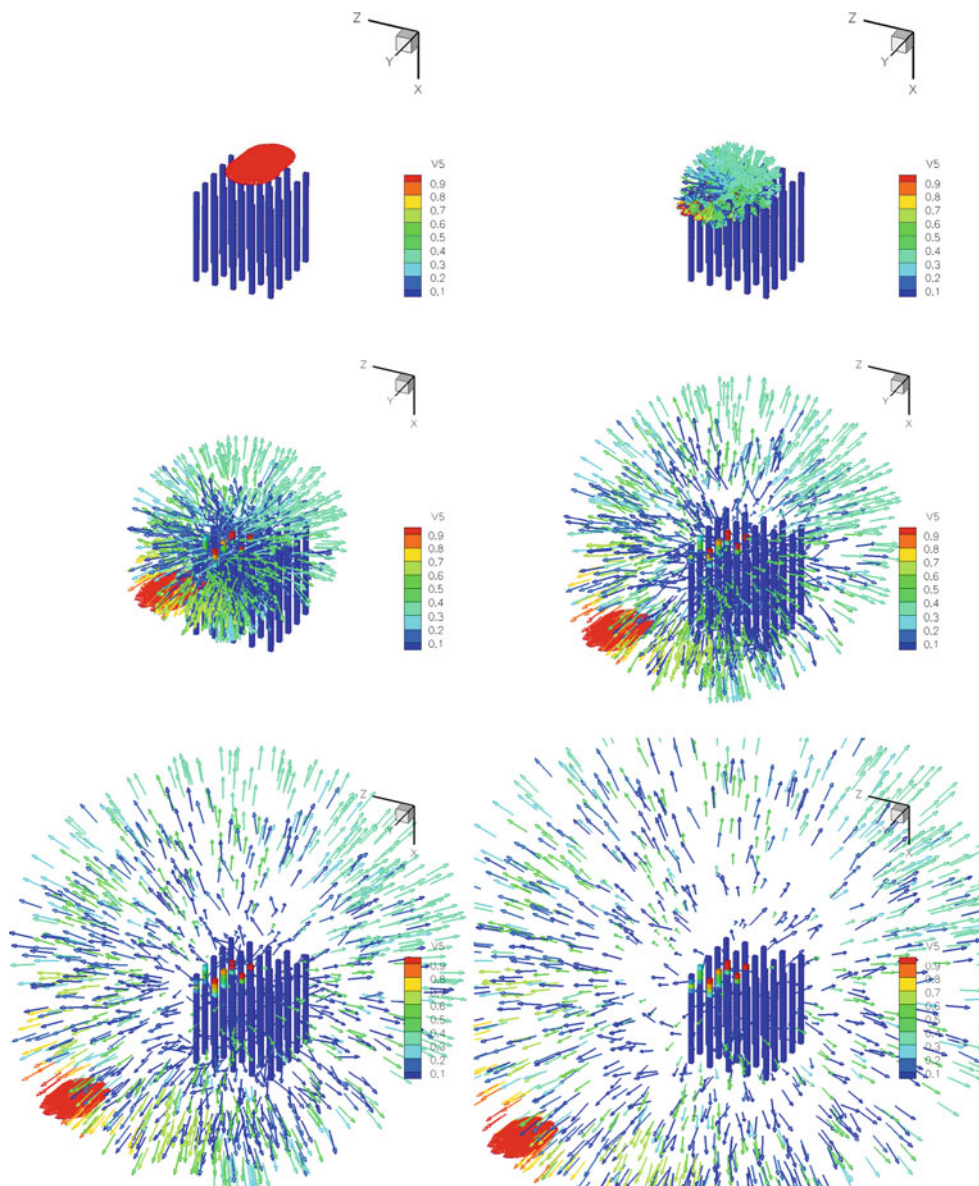


Fig. 8 Starting from *left to right* and *top to bottom*, the progressive movement of rays (initially with inclined angle of incidence $\nu(t = 0) = c(\cos \frac{\pi}{4}, \sin \frac{\pi}{4}, 0)$) comprising a beam. The *color of the vectors* indicate

the irradiance, while the *color of the rods* indicate the absorption of the irradiant energy

comprise a wide variety of high-performance structures, such as automobiles and aircraft. Finally, the “tuned/functionalized” energy-absorption properties of materials in the photovoltaic industry by surface deposition of rod-like material is now starting to generate large interest in the materials community (Kelzenberg et al. [7] and Garnett and Yang [3]). The use of the presented analysis for all of the mentioned applications is under current investigation by the author.

Appendix: Geometrical ray theory

Following a somewhat classical analysis found in, for example, Elmore and Heald [2], Cerveny et al. [1] and others, we

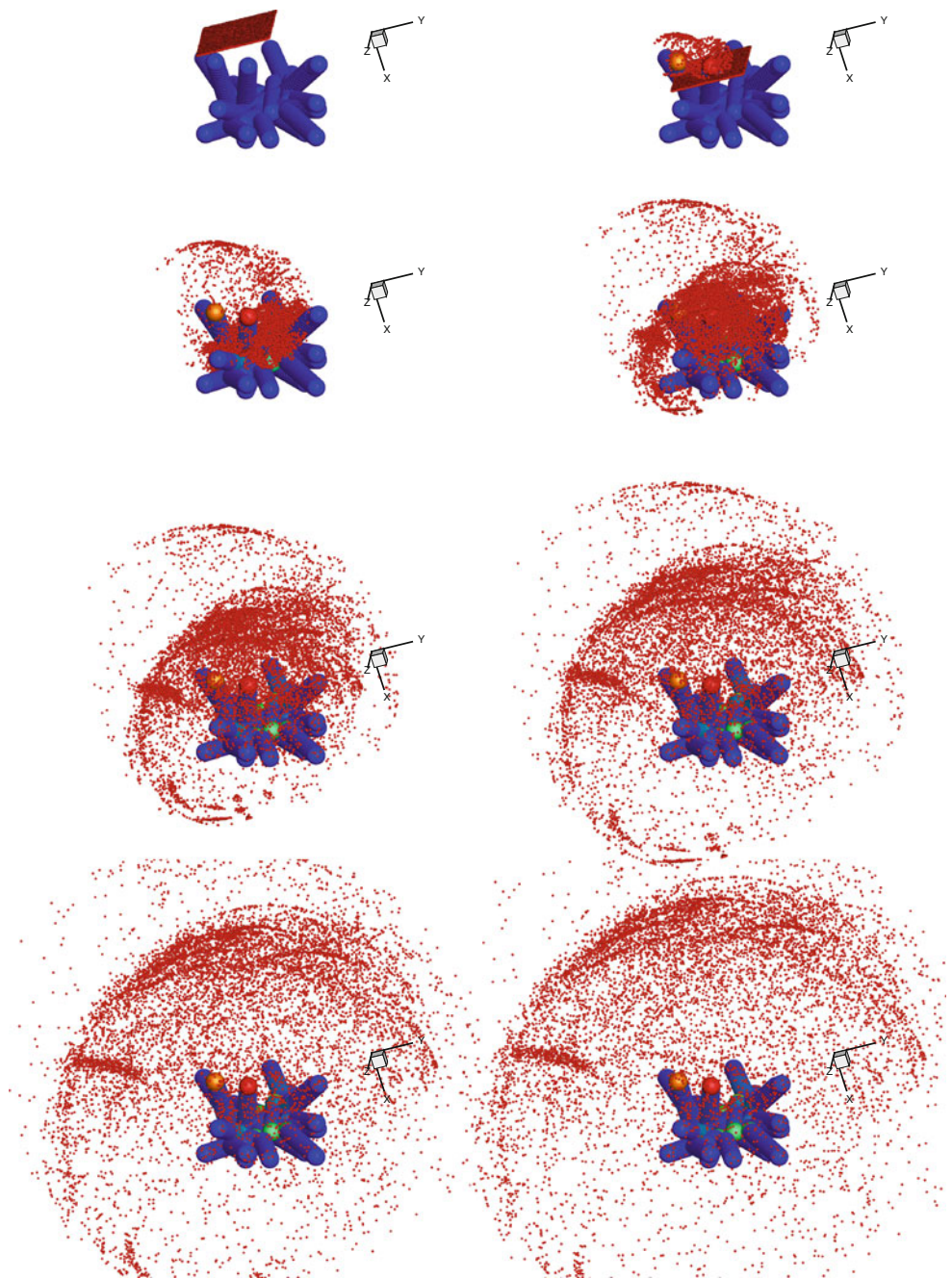
consider the propagation of a general disturbance, ψ , governed by a generic wave equation:

$$\nabla^2 \psi = \frac{1}{c^2(\mathbf{x})} \frac{\partial^2 \psi}{\partial t^2}. \tag{7.1}$$

Here $c(\mathbf{x})$ is a spatially varying wave speed corresponding to a general inhomogeneous medium, where $c(\mathbf{x}) = c_o$ in a homogeneous reference medium and where the refractive index is defined as $n = c_o/c(\mathbf{x})$. Consider a trial solution of the form

$$\psi(\mathbf{x}, t) = A(\mathbf{x})e^{j(k_o S(\mathbf{x}) - \omega t)}, \tag{7.2}$$

Fig. 9 Starting from *left to right* and *top to bottom*, the progressive movement of rays (initially with direct angle of incidence $\mathbf{v}(t = 0) = (c, 0, 0)$) comprising a beam. The vectors were removed to clearly see the energy absorption of the surface



where $A(\mathbf{x})$ is the amplitude of the disturbance, and where $k_o = \omega/c_o = 2\pi/\lambda$ is the wave number in the reference medium. The function $S(\mathbf{x})$ (dimensions of length) is known as the “Eikonal”, which in Greek means “image”. One can interpret a set of waves as simply a family of surfaces for which the values of $k_o S(\mathbf{x})$ differ in increments of 2π . Substituting the trial solution into the wave equation, one obtains

$$k_o^2 A(n^2 - \nabla S \cdot \nabla S) + j k_o (2\nabla A \cdot \nabla S + A \nabla^2 S) + \nabla^2 A = 0. \tag{7.3}$$

There are a variety of arguments to motivate so-called “Ray Theory”. Probably the simplest is simply to require that, as $k_o \rightarrow \infty$, each of the k_o -terms, the zeroth-order k_o -term, the first-order k_o -term and the second-order k_o -term, must vanish. Applying this requirement to the second-order k_o -term yields

$$n^2 = \nabla S \cdot \nabla S = \|\nabla S\|^2. \tag{7.4}$$

For a uniform medium, $n = \text{const}$, provided $\nabla^2 A = 0$ and an initial plane wave surface $S = \text{const}$, then Eq. 7.3 implies

$$S(\mathbf{x}) = n(\alpha x + \beta y + \phi z), \tag{7.5}$$

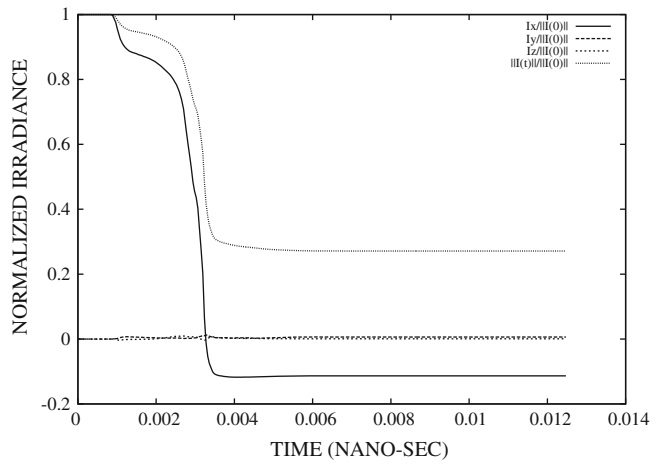
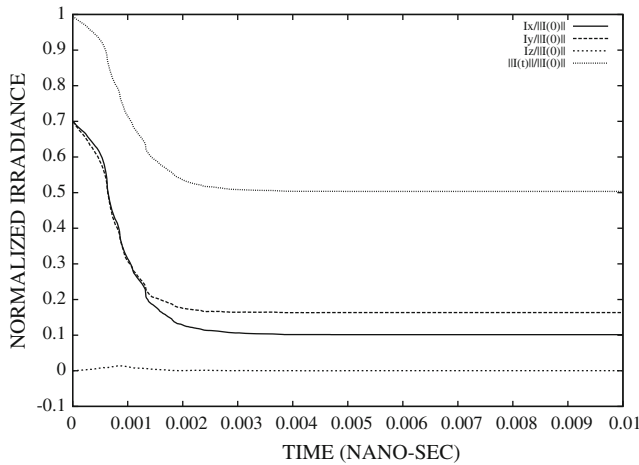


Fig. 10 The aggregate components of the irradiance vectors in the ray system. *Left* the energy content for the system for the aligned-rod system. *Right* the energy content for the system for the misaligned-rod system. Much more energy is reflected backwards for the misaligned

case. At steady-state, 50% of the energy has been absorbed by the aligned system (initially with inclined angle of incidence $\nu(t = 0) = c(\cos \frac{\pi}{4}, \sin \frac{\pi}{4}, 0)$) and approximately 75% by the misaligned system (initially with direct angle of incidence $\nu(t = 0) = (c, 0, 0)$)

where α , β and ϕ are direction cosines. More generally, when $n \neq 0$, then Eq. 7.4 implies

$$\nabla S(\mathbf{x}) = n(\mathbf{x})\hat{s}(\mathbf{x}), \tag{7.6}$$

where $\hat{s}(\mathbf{x})$ is a unit (direction) vector.

From elementary calculus, recall that ∇S is perpendicular to $S = const$. This allows for the natural definition of continuous curves, called rays, that are everywhere parallel to the local direction $\hat{s}(\mathbf{x})$. Rearranging first-order k_o -term of Eq. 7.3

$$\frac{1}{A} \nabla A \cdot \nabla S = -\frac{1}{2} \nabla^2 S = -\frac{1}{2} \nabla \cdot (n\hat{s}). \tag{7.7}$$

Recalling the directional derivative, $\frac{d(\cdot)}{ds} \stackrel{\text{def}}{=} \hat{s} \cdot \nabla(\cdot)$, we have

$$\left(\frac{\nabla S}{\|\nabla S\|} \right) \cdot \nabla A = \left(\frac{\nabla S}{n} \right) \cdot \nabla A = \frac{dA}{ds}, \tag{7.8}$$

where s is the arc-length coordinate along the ray. With this definition, once $S(\mathbf{x})$ is known, the component of ∇A in the $\hat{s}(\mathbf{x})$ can be found from Eqs. 7.7 and 7.8:

$$\frac{1}{A} \frac{dA}{ds} = -\frac{1}{2n} \nabla \cdot (n\hat{s}). \tag{7.9}$$

Thus, we are able to determine how the amplitude of the trial solution changes along a ray, but not perpendicular to the trajectory.

Geometrical “ray-tracing”, deals directly with the ray trajectories, rather than finding them as a by-product of the solution of the wave equation for the Eikonal function S and the resulting wave front. To eliminate S we need to look at the rate of change of the quantity $n\hat{s}$ along the ray. Making repeated use of Eq. 7.6, we have

$$\begin{aligned} \frac{d(n\hat{s})}{ds} &= \hat{s} \cdot \nabla(\nabla S) = \frac{\nabla S}{n} \cdot \nabla(\nabla S) \\ &= \frac{1}{2n} \nabla(\nabla S \cdot \nabla S) = \frac{1}{2n} \nabla n^2 = \nabla n, \end{aligned} \tag{7.10}$$

where $\frac{d(\cdot)}{ds} \stackrel{\text{def}}{=} \hat{s} \cdot \nabla(\cdot)$. The previous equation allows us to find the trajectories of a ray (\hat{s}), given only the refractive index $n(\mathbf{x})$ and the initial direction \hat{s}_i of the desired ray.

Remark A more general derivation of the eikonal equation can be found in a variety of textbooks, for example, Cervený et al. [1], and starts by assuming a trial solution of the form

$$\psi(\mathbf{x}, t) = A(\mathbf{x})\Phi(t - \Lambda(\mathbf{x})) \tag{7.11}$$

where Λ is an eikonal function, and the waveform function α is assumed to be of high frequency.⁶ This function is then substituted into the wave equation to yield

$$\nabla^2 A \Phi + 2\nabla A \cdot \nabla \Phi + A \nabla^2 \Phi = \frac{1}{c^2} A \frac{\partial^2 \Phi}{\partial t^2}. \tag{7.12}$$

After using the chain rule of differentiation, this can be written as

$$\begin{aligned} \frac{\partial^2 \Phi}{\partial \Lambda^2} A \left(\nabla \Lambda \cdot \nabla \Lambda - \frac{1}{c^2} \right) + \frac{\partial \Phi}{\partial \Lambda} \left(2\nabla A \cdot \nabla \Lambda + A \nabla^2 \Lambda \right) \\ + \Phi \nabla^2 A = 0. \end{aligned} \tag{7.13}$$

Analogous to the special case considered before, to motivate so-called “Ray Theory” one requires that the coefficients of

⁶ This is a more general case than the one considered in Eq. 7.2 where $\Phi(t - \Lambda(\mathbf{x})) = e^{j(k_o S(\mathbf{x}) - \omega t)}$.

$\frac{\partial^2 \Phi}{\partial \Lambda^2}$, $\frac{\partial \Phi}{\partial \Lambda}$ and Φ are satisfied separately, in other words, the following hold

$$\nabla \Lambda \cdot \nabla \Lambda - \frac{1}{c^2} = 0 \quad (7.14)$$

and

$$2\nabla A \cdot \nabla \Lambda + A\nabla^2 \Lambda = 0 \quad (7.15)$$

and

$$\nabla^2 A = 0. \quad (7.16)$$

References

1. Cerveny V, Molotkov IA, Psencik I (1977) Ray methods in seismology. Univerzita Karlova, Praha
2. Elmore WC, Heald MA (1985) Physics of waves. Dover Publications re-issue, New York
3. Garnett E, Yang P (2010) (eds) Light trapping in silicon nanowire solar cells. *Nanoletters* 10:1082–1087
4. Gross H (2005) Handbook of optical systems. In: Gross H (ed) Fundamental of technical optics. Wiley, Weinheim
5. Guenther K (1990) Revisiting structure-zone models for thin-film growth. *SPIE* 1324:2
6. Hawkeye M, Brett MJ (2007) Glancing angle deposition: fabrication, properties, and applications of micro- and nanostructured thin films. *J Vac Sci Technol A* 25(5):1317
7. Kelzenberg MD, Buettcher SW, Petykiewicz JA, Turner-Evans DB, Putnam MC, Warren EL, Spurgeon JM, Briggs RM, Lewis NS, Attwater HA (2010) Enhanced absorption and carrier collection in Si wire arrays for photovoltaic applications. *Nat Mater* 9:239–244
8. Macleod HA (2001) Thin film optical filters, 3rd edn. I. O. P., Bristol
9. Martin P (2009) Handbook of deposition technologies for films and coatings, 3rd edn. Elsevier, Canada
10. Martin P (2011) Introduction to surface engineering and functionally engineered materials. Scrivener and Elsevier, Amsterdam
11. Messier R, Giri AP, Roy R (1984) Revised structure zone for thin film physical structure. *J Vac Sci Technol A* 2(2):500
12. Pöschel T, Schwager T (2004) Computational granular dynamics. Springer, New York
13. Preciado JA, Rubinsky B, Otten D, Nelsen B, Martin M, Greif R (2002) Radiative properties of polar bear hair. *ASME, BED-Vol* 53. *Advances in Bioengineering*, pp 1–2
14. Stamm RF, Garcia ML, Fuchs JJ (1977) The optical properties of human hair-I. Fundamental considerations and goniophotometer curves. *J Cosmet Chem* 28:571–599
15. Zohdi TI (2006) On the optical thickness of disordered particulate media. *Mech Mater* 38:969–981
16. Zohdi TI (2006) Computation of the coupled thermo-optical scattering properties of random particulate systems. *Comput Methods Appl Mech Eng* 195:5813–5830
17. Zohdi TI, Kuypers FA (2006) Modeling and rapid simulation of multiple red blood cell light scattering. *Proc R Soc Interface* 3(11):823–831
18. Zohdi TI (2007) Introduction to the modeling and simulation of particulate flows. SIAM (Society for Industrial and Applied Mathematics), Philadelphia